# Determination of the quasi-TE mode (*in-plane*) graphene linear absorption coefficient *via* integration with silicon-on-insulator racetrack cavity resonators

**Iain F Crowe,[1,*] Nick Clark,[2] Siham Hussein,[1] Brian Towlson,[1] Eric Whittaker,[1] Milan M Milosevic,[3,§] Frederic Y Gardes,[3] Goran Z Mashanovich,[3] Matthew P Halsall[1] and Aravind Vijayaraghavan[2]**

[1]*Photon Science Institute and School of Electrical and Electronic Engineering, University of Manchester, Oxford Road, Manchester M13 9PL, UK*
[2]*School of Materials, University of Manchester, Oxford Road, Manchester M13 9PL, UK*
[3] *Optoelectronics Research Centre, University of Southampton, SO17 1BJ, UK*
[§]*now at Etaphase, Inc., Bellevue, WA, USA*
[*]*iain.crowe@manchester.ac.uk*

**Abstract:** We examine the near-IR light-matter interaction for graphene integrated cavity ring resonators based on silicon-on-insulator (SOI) race-track waveguides. Fitting of the cavity resonances from quasi-TE mode transmission spectra reveal the real part of the effective refractive index for graphene, $n_{\text{eff}} = 2.23 \pm 0.02$ and linear absorption coefficient, $\alpha_{\text{gTE}} = 0.11 \pm 0.01 \text{dB}\mu\text{m}^{-1}$. The evanescent nature of the guided mode coupling to graphene at resonance depends strongly on the height of the graphene above the cavity, which places limits on the cavity length for optical sensing applications.



**OCIS codes:** (240.0240) Optics at surfaces; (240.0310) Thin films; (240.6490) Spectroscopy, surface.

## References and links

1. K. S. Novoselov, V. I. Fal'ko, L. Colombo, P. R. Gellert, M. G. Schwab, and K. Kim, "A roadmap for graphene," Nature **490**(7419), 192–200 (2012).
2. M. Liu, X. Yin, E. Ulin-Avila, B. Geng, T. Zentgraf, L. Ju, F. Wang, and X. Zhang, "A graphene-based broadband optical modulator," Nature **474**(7349), 64–67 (2011).
3. K. Kim, J. Y. Choi, T. Kim, S. H. Cho, and H. J. Chung, "A role for graphene in silicon-based semiconductor devices," Nature **479**(7373), 338–344 (2011).
4. D. J. Thomson, F. Y. Gardes, J.-M. Fedeli, S. Zlatanovic, Y. Hu, B. P. P. Kuo, E. Myslivets, N. Alic, S. Radic, G. Z. Mashanovich, and G. T. Reed, "50-Gb/s silicon optical modulator," IEEE Photon. Technol. Lett. **24**(4), 234–236 (2012).
5. G. Li, X. Zheng, J. Yao, H. Thacker, I. Shubin, Y. Luo, K. Raj, J. E. Cunningham, and A. V. Krishnamoorthy, "25Gb/s 1V-driving CMOS ring modulator with integrated thermal tuning," Opt. Express **19**(21), 20435–20443 (2011).
6. W. Bogaerts, P. De Heyn, T. Van Vaerenbergh, K. De Vos, S. K. Selvaraja, T. Claes, P. Dumon, P. Bienstman, D. Van Thourhout, and R. Baets, "Silicon microring resonators," Laser and Photonics Reviews **6**(1), 47–73 (2012).
7. M. K. Park, J. S. Kee, J. Y. Quah, V. Netto, J. Song, Q. Fang, E. M. La Fosse, and G.-Q. Lo, "Label-free aptamer sensor based on silicon microring resonators," Sens. Actuators B Chem. **176**, 552–559 (2013).
8. M. Iqbal, M. A. Gleeson, B. Spaugh, F. Tybor, W. G. Gunn, M. Hochberg, T. Baehr-Jones, R. C. Bailey, and L. C. Gunn, "Label-free biosensor arrays based on silicon ring resonators and high-speed optical scanning instrumentation," IEEE J. Sel. Top. Quantum Electron. **16**(3), 654–661 (2010).
9. C. Ciminelli, F. Dell'Olio, D. Conteduca, C. M. Campanella, and M. N. Armenise, "High performance SOI microring resonator for biochemical sensing," Opt. Laser Technol. **59**, 60–67 (2014).
10. J. E. Moses and A. D. Moorhouse, "The growing applications of click chemistry," Opt. Express **19**(21), 20435–20443 (2011).
11. H.-Y. Chen, M. Hirtz, X. Deng, T. Laue, H. Fuchs, and J. Lahann, "Substrate-independent dip-pen nanolithography based on reactive coatings," J. Am. Chem. Soc. **132**(51), 18023–18025 (2010).

#212944 - $15.00 USD Received 27 May 2014; revised 7 Jul 2014; accepted 8 Jul 2014; published 25 Jul 2014

12. X. Li, W. Cai, J. An, S. Kim, J. Nah, D. Yang, R. Piner, A. Velamakanni, I. Jung, E. Tutuc, S. K. Banerjee, L. Colombo, and R. S. Ruoff, "Large-area synthesis of high-quality and uniform graphene films on copper foils," Science **324**(5932), 1312–1314 (2009).
13. H. Wang, Y. Wang, X. Cao, M. Feng, and G. Lan, "Vibrational properties of graphene and graphene layers," J. Raman Spectrosc. **40**(12), 1791–1796 (2009).
14. K. Kim, S. Coh, L. Z. Tan, W. Regan, J. M. Yuk, E. Chatterjee, M. F. Crommie, M. L. Cohen, S. G. Louie, and A. Zettl, "Raman spectroscopy study of rotated double-layer graphene: misorientation-angle dependence of electronic structure," Phys. Rev. Lett. **108**(24), 246103 (2012).
15. V. M. Menon, W. Tong, and S. R. Forrest, "Control of quality factor and critical coupling in microring resonators through integration of a semiconductor optical amplifier," IEEE Photon. Technol. Lett. **16**(5), 1343–1345 (2004).
16. J. Niehusmann, A. Vörckel, P. H. Bolivar, T. Wahlbrink, W. Henschel, and H. Kurz, "Ultrahigh-quality-factor silicon-on-insulator microring resonator," Opt. Lett. **29**(24), 2861–2863 (2004).
17. L. Prechtel, L. Song, D. Schuh, P. Ajayan, W. Wegscheider, and A. W. Holleitner, "Time-resolved ultrafast photocurrents and terahertz generation in freely suspended graphene," Nat Commun **3**, 646 (2012).
18. I. Jung, M. Pelton, R. Piner, D. A. Dikin, S. Stankovich, S. Watcharotone, M. Hausner, and R. S. Ruoff, "Simple approach for high-contrast optical imaging and characterization of graphene-based sheets," Nano Lett. **7**(12), 3569–3575 (2007).
19. Z. H. Ni, H. M. Wang, J. Kasim, H. M. Fan, T. Yu, Y. H. Wu, Y. P. Feng, and Z. X. Shen, "Graphene thickness determination using reflection and contrast spectroscopy," Nano Lett. **7**(9), 2758–2763 (2007).
20. P. Blake, E. W. Hill, A. H. Castro Neto, K. S. Novoselov, D. Jiang, R. Yang, T. J. Booth, and A. K. Geim, "Making graphene visible," Appl. Phys. Lett. **91**(6), 063124 (2007).
21. Z. Lu and W. Zhao, "Nanoscale electro-optic modulation based on graphene-slot waveguides," J. Opt. Soc. Am. B **29**(6), 1490–1496 (2012).
22. R. Kou, S. Tanabe, T. Tsuchizawa, K. Warabi, S. Suzuki, H. Hibino, H. Nakajima, and K. Yamada, "Characterization of optical absorption and polarization dependence of single-layer graphene integrated on a silicon wire waveguide," Jpn. J. Appl. Phys. **52**(6R), 060203 (2013).
23. H. Li, Y. Anugrah, S. J. Koester, and M. Li, "Optical absorption in graphene integrated on silicon waveguides," Appl. Phys. Lett. **101**(11), 111110 (2012).
24. R. Kou, S. Tanabe, T. Tsuchizawa, T. Yamamoto, H. Hibino, H. Nakajima, and K. Yamada, "Influence of graphene on quality factor variation in a silicon ring resonator," Appl. Phys. Lett. **104**(9), 091122 (2014).
25. Q. Bao, H. Zhang, B. Wang, Z. Ni, C. H. Y. X. Lim, Y. Wang, D. Y. Tang, and K. P. Loh, "Broadband graphene polarizer," Nat. Photonics **5**(7), 411–415 (2011).

## 1. Introduction

The disruptive technological potential of graphene is extremely wide ranging [1], with the emergence of the first commercial devices anticipated as early as 2015. In particular, graphene's ability to absorb light over an extremely wide (UV to IR) wavelength range, coupled with its high carrier mobility offer the potential for a plethora of photonic devices including ultrafast, high band-width photo-detectors and optical modulators [2]. On the other hand, as a true 2D material, it has an extremely large surface area, which combined with its chemical purity, reactivity and simplicity of functionalization make for an ideal sensing platform that could lead to ultra-sensitive devices for the detection of biological and/or gas molecules in fields as diverse as healthcare, environment and homeland security.

However, there are certain fundamental limitations associated with graphene when compared with conventional semiconductors. For instance, intrinsic graphene is a semi-metal (zero band-gap semiconductor) which means that it exhibits a poor 'on/off' current ratio when integrated into electronic devices [3]. This, coupled with the huge financial and intellectual investment in the silicon CMOS micro-electronics industry and, more recently, the emerging field of silicon photonics, means that graphene is unlikely to completely supersede silicon in the foreseeable future. Rather, there are distinct and obvious advantages to be gained by combining these two power-house material systems. For instance, despite its large operating bandwidth, the relatively small fraction of photons absorbed at normal incidence (2.3%) and the small effective detection area of defect-free graphene limits its responsivity to levels well below that required for a commercial photo-detector [1]. However, by integrating graphene with a silicon waveguide, the light–matter (graphene) interaction length and therefore optical absorption can be increased considerably [3]. And the relationship is bi-lateral; for instance, integrating graphene with current commercial silicon optical modulators, such as the Mach-Zehnder Interferometer (MZI) [4] and the cavity ring resonator [5], which are used to encode transmission data for optical interconnects, offers the potential to improve device

#212944 - $15.00 USD Received 27 May 2014; revised 7 Jul 2014; accepted 8 Jul 2014; published 25 Jul 2014

performance precisely because of graphene's ultra-fast response over an extremely broad spectral range.

Whatever the application, understanding the nature of the light-matter interaction in graphene integrated silicon photonic devices is critical if the combined potential 'greater than the sum of its parts' is to be realized.

Our immediate focus is trying to understand the limitations on the practical sensitivity of silicon photonic cavities, in which graphene acts as a sensitization layer or pre-concentrator with improved reactivity over the silicon surface, for sensing applications. The ring resonator is one such cavity, in which the wavelength specific mode confinement of light arises from the high refractive index contrast at the silicon/air interface. Such cavity resonators are routinely fabricated, *via* deep UV or e-beam lithography with sub-μm precision, from the commercial silicon-on-insulator (SOI) platform with a wire-ring, positioned adjacent to a straight section wire-waveguide, providing a low loss resonant cavity into which light is evanescently coupled when the wavelength matches an integer number of round-trips of the ring [6]. The efficiency with which this coupling is achieved, and the very narrow (sub-nm) cavity resonances, provides a tightly confined (both physically and spectrally) intense evanescent field for near-surface molecular interaction, and therefore sensing [7–9]. The transmission spectrum (of a tuneable laser or broadband source) at the wire-guide output reveals these cavity resonances, the spectral position of which is also a strong function of the local (near surface) refractive index, which depends on the concentration of the bound target molecule. By monitoring this transmitted light intensity it is therefore possible to detect extremely small changes in the refractive index of the near surface region as molecules attach themselves to the primed silicon cavity surface. The functionalization of such silicon micro-cavities for bio-sensing applications has now been reasonably well explored, for instance for the detection of single-stranded DNA by peptide nucleic acid functionalization [7], streptavidin detection by biotin functionalization [8] and glucose detection by glucose oxidase functionalization [9]. However, the chemical functionalisation of silicon is limited in its scope due to its relatively poor reactivity, so that even the versatile 'click-chemistry' route to bio-functionalization [10] is not possible directly on silicon. Whilst methods to improve the reactivity of silicon surfaces, such as coating with poly-p-xylylenes have been described [11], these still leave a relatively thick (μm-scale) coating on the surface. For waveguide based photonic sensors such as these, the evanescent field decays exponentially away from the surface, and therefore it is essential that the reactive groups (be they biological or gaseous molecular compounds) be located as close to the silicon surface as possible and thus relatively thick coatings are undesirable. Rather, our approach is to coat our cavity surfaces with monolayer graphene with the expectation that the highly versatile reactivity of graphene will open up a wide variety of sensing applications that would otherwise be inaccessible to purely silicon photonic platforms. As a first step in this process, in this contribution we report measurement of the optical response of graphene coated cavities and in so doing determine both the real part of the effective refractive index and the quasi-TE (*in-plane*) linear absorption coefficient for single layer graphene.

## 2. Experimental details

Strip waveguides and racetrack resonators with height of 220nm and width of w = 350nm were fabricated, from commercial SOI with a 2μm thick buried oxide layer, via deep UV (193nm) lithography using standard complementary metal-oxide semiconductor fabrication processes. Three racetrack resonators, with equivalent racetrack-to-wire coupling length, $L_c$ = 13μm and coupling gap, g = 0.3μm but different radii of curvature, r = 10, 20 and 40μm are reported here, with only the smaller devices integrated with graphene.

The graphene was grown by chemical vapour deposition (CVD) on copper foils (Gratome-R-Cu, Bluestone Global Tech) and transferred on to the SOI wafer containing the devices using a polymer-mediated wet transfer procedure described elsewhere [12]. The graphene was patterned, to ensure selective coverage of the racetrack resonators, using raster-scan photolithography and oxygen plasma etching. The sample was subsequently cleaned

#212944 - $15.00 USD Received 27 May 2014; revised 7 Jul 2014; accepted 8 Jul 2014; published 25 Jul 2014

with acetone and annealed at 270°C in a reducing atmosphere to remove residual photo-resist contamination. In order to confirm we have deposited single layer graphene, we have used Raman scattering spectroscopy. The samples were excited with a 514nm (Cobolt Fandango solid state diode) laser via a 50x microscope objective lens and the *Raman* spectra (not shown here) collected in a back-scattering geometry, dispersed in a Renishaw 1000 micro-Raman system and detected using a charge coupled device (CCD) camera. Three key factors from the scattering spectra may be used to determine whether graphene is single ($n$ = 1) or multi- ($n$ = 2, 3, 4…) layer; the G-peak position, $\omega_G$ ($n$) = 1581.6 + 11/(1 + $n^{1.6}$) [13], the width ($w_{2D}$) and symmetry of the 2D-peak and the ratio of the 2D and G integrated intensities, $I_{2D}/I_G$ [14]. From Lorentzian fits to our measured G and 2D scattering peaks, we obtain $\omega_G$ ($n$ = 1) = 1587.2 ± 0.1cm$^{-1}$, a symmetric 2D peak with width, $w_{2D}$ = 28cm$^{-1}$ and $I_{2D}/I_G$ ~6, all of which confirm we have single layer graphene.

In order to facilitate optical device characterization in a sensing environment, we have developed a novel system, Fig. 1 for achieving free-space delivery and collection of the optical signal from an external cavity laser (Thorlabs TLK-L1550R), which has a narrow (100kHz) linewidth and tuning range from 1480 to 1600nm.

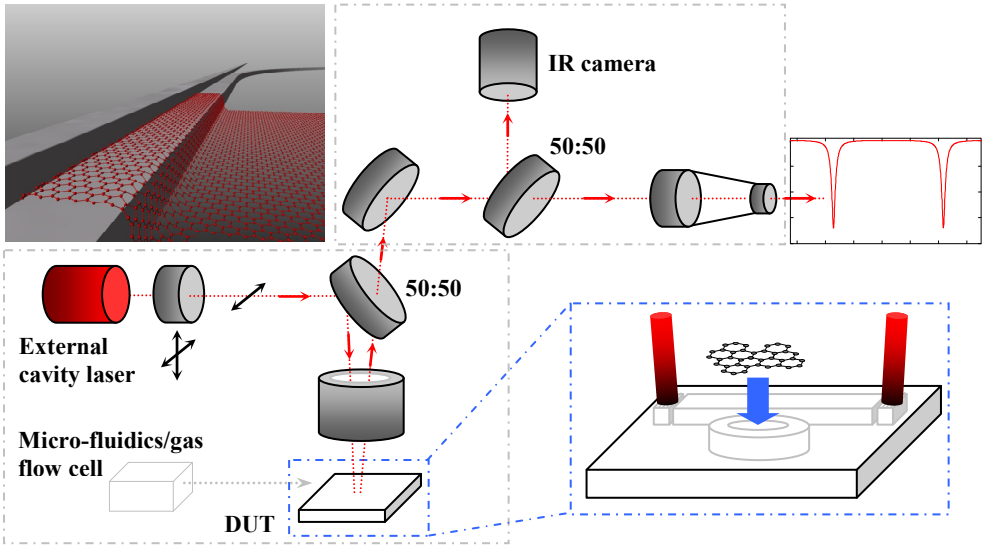


Fig. 1. (a) Schematic of the graphene integrated race-track resonator; The image illustrates the selective (partial) coverage of the race-track at the coupling section with the un-coated wire-guide (b) free-space optical set-up for measuring the resonator device transmission characteristics

The laser output is delivered, *via* a single mode fiber and polarizer, to a 50:50 beam-splitter, where it is reflected at near (~11°) normal incidence onto a wide field of view, long working distance 5x microscope objective lens (Thorlabs LMS03-BB). Unlike the fiber based techniques for characterization of such devices, this arrangement provides a 'stand-off' optical system (of ~3cm) above our device under test for future integration of micro-fluidic channels and/or gas flow cell. The laser spot is focused onto a surface grating (optimized for TE mode coupling) at one end of the strip waveguide, which tapers over ~1mm to achieve single-guided mode operation. The total length of the strip waveguide is ~3mm at the end of which the light emerges, *via* another tapering section and equivalent surface grating, at a similar angle off the normal. The light is then collected using the same objective lens and passes through the other side of the beam-splitter, whereupon it is reflected from a mirror onto a second beam-splitter, dividing the collected light between the aperture of an IR camera, which is used to image the waveguide input and output for alignment, and a fiber-coupler, which focuses the light onto the end of a fiber where it is delivered to a bench-top,

#212944 - $15.00 USD Received 27 May 2014; revised 7 Jul 2014; accepted 8 Jul 2014; published 25 Jul 2014

*Bayspec* SuperGamut© spectrometer with thermo-electrically cooled InGaAs array detector from which we determine the transmitted light intensity as a function of wavelength. The transmission spectra are all corrected for spectral variations in the laser output power and waveguide insertion loss.

### 3. Results and discussion

A typical transmission spectrum for the race-track ring resonator device (r = 40μm) without graphene is shown in Fig. 2.

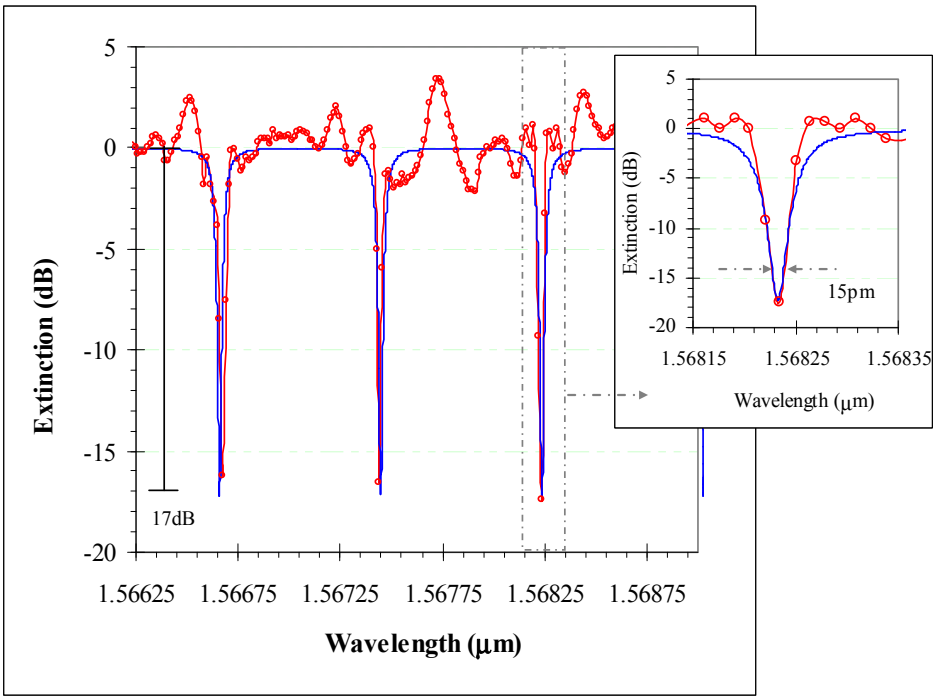


Fig. 2. Measured (red) transmission spectrum for a silicon racetrack cavity resonator (physical dimensions, r = 40μm and $L_c$ = 13μm) without graphene. The model (blue) curve is derived from a fit using Eq. (1) with r = 42.5μm, $L_c$ = 14μm, α = 1.737dBcm$^{-1}$ and $n_{eff}$ = 3.249. Inset: close-up of the resonance peak around 1.56825nm

The device exhibits a relatively high extinction (~17dB) on resonance with a quality factor ($Q = \lambda_0/\Delta\lambda$) of the order of $10^5$. The measured transmission spectrum is well described by the following expression, modified after [15]:

$$T\left(\lambda, L, n_{eff}, \alpha\right) = \left(1-\gamma\right)\left[\frac{\left(\sqrt{1-k}\right)-\left(\sqrt{1-\gamma}\right)e^{-\alpha\frac{\left(Ln_{eff}\right)}{2}-i\left(2\pi n_{eff}^2\frac{L}{\lambda}\right)}}{1-\left(\sqrt{1-\gamma}\right)\left(\sqrt{1-k}\right)e^{-\alpha\frac{\left(Ln_{eff}\right)}{2}-i\left(2\pi n_{eff}^2\frac{L}{\lambda}\right)}}\right]^2 \qquad (1)$$

Where k and γ are respectively power coupling and intensity loss factors, which depend on the coupling efficiency of the ring resonator structure, L ( = 2πr + 2$L_c$) is the total physical round-trip length of the racetrack waveguide with radius of curvature, r and coupling length, $L_c$. $n_{eff}$ is the effective refractive index and α is the loss coefficient, which includes contributions from both scattering and absorption. The model values obtained from the fit for r and $L_c$ agree well with the design (and known physical) dimensions of the racetrack and the

#212944 - $15.00 USD Received 27 May 2014; revised 7 Jul 2014; accepted 8 Jul 2014; published 25 Jul 2014

values for $n_{eff}$ and α are in excellent agreement with literature values [16] for this type of device.

Figure 3 shows typical transmission spectra for the two graphene integrated racetracks with different radius of curvature (r = 10 and 20μm) but otherwise identical physical parameters ($L_c$, g and w) to the device without graphene.

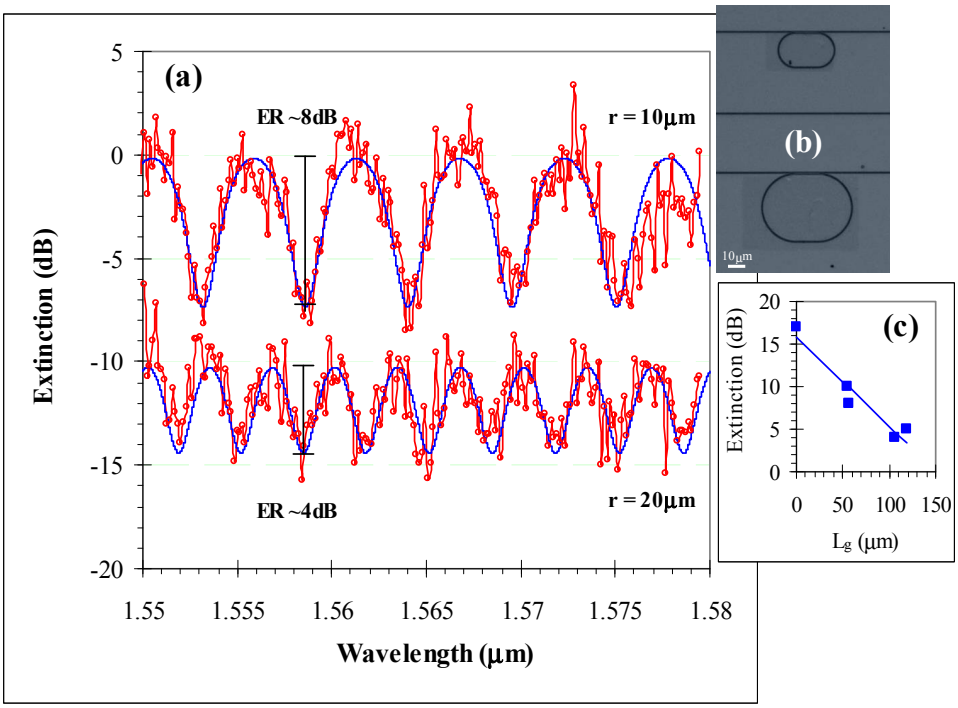


Fig. 3. (a) Measured (red) and modelled (Eq. (1), blue) transmission spectra (offset for clarity). Fits to both data sets yield residual minima with physical dimensions r = 10, 20μm and $L_c$ = 13μm, $n_{eff}$ = 2.23 ± 0.02 and α = 0.11dBμm$^{-1}$ (b) Optical images of the two corresponding, selectively coated graphene integrated silicon racetrack cavity resonators with (top) r = 10μm and (bottom) r = 20μm. (c) Measured peak extinction as a function of the light-matter (graphene) interaction length, $L_g$ with linear regression fit of the form $ER(L_g)_{dB} = ER(0)_{dB} - \alpha L_g$ with slope α = 0.104dBμm$^{-1}$

Figure 3 reveals a good fit to the transmission spectra using Eq. (1) for both cavity lengths with an effective refractive index, $n_{eff}$ = 2.23 ± 0.02. It is important to stress here that $n_{eff}$ is representative of the waveguide core and cladding material and it is not trivial to extract a precise value for the refractive index of graphene, $n_g$ from this. Published values for $n_g$ [17–19] tend to be somewhat higher than that of graphene oxide and lower than that of bulk graphite [20].

The large variation we obtain in $n_{eff}$, going from un-coated to graphene coated cavities indicates dramatically altered modal propagation in our system and suggests that the optical properties, including the index of refraction are dominated by the graphene. Whilst $n_{eff}$ can be expected to vary to a lesser degree according to the exact cavity dimensions, which determine the mode profile, we note that the value we have obtained here is in good agreement with previously reported values for modelled graphene-slot waveguides integrated into silicon platforms [21].

In general, although ring resonator scattering losses tend to increase with smaller ring radii, this should be balanced by lower propagation losses due to the smaller overall round-trip length. In the case of the graphene integrated devices we have measured, variation in the scattering losses due to tighter bend radii are negligible and the losses leading to the significant reduction of the extinction ratio and broadening of the resonances observed in Fig.

#212944 - $15.00 USD Received 27 May 2014; revised 7 Jul 2014; accepted 8 Jul 2014; published 25 Jul 2014

3 are almost entirely the result of increased propagation loss (absorption) in the graphene layer situated at the cavity surfaces. These losses are a strong function of the light-matter (graphene) interaction length, $L_g$ and so as the racetrack size increases the observed extinction diminishes. Thus by examining the change in the peak extinction ratio for different overall graphene integrated racetrack lengths, one can independently determine the absorption coefficient for graphene and cross-correlate this with the value obtained by fitting the resonance spectra with Eq. (1). A total of four graphene integrated devices (two with r = 10μm and two with r = 20μm) were measured and their extinction ratio is plotted as a function of $L_g$, along with the data point for the no graphene device, in **Fig. 3(c)**. Analysis of the optical images in Fig. 3(b) revealed that the rings were not completely coated by the graphene and so $L_g$ has been corrected for this fractional coverage, n ( = $L_g$/L; 0 < n < 1). A linear regression fit to the data in Fig. 3(c), of the form $ER(L_g)_{dB} = ER(0)_{dB} - \alpha L_g$, yields a value for the graphene linear absorption coefficient, $\alpha = 0.104 dB\mu m^{-1}$, which is equivalent (within experimental error) to the value derived from the fitting of Eq. (1) to the transmission spectra in Fig. 3(a). We note that similar analyses were recently reported for graphene integrated silicon wire waveguides without cavities [22], graphene integrated MZI devices [23] and from analysis of the Q-factor variation for a single ring resonator, partially coated with graphene [24], all of which yield similar values of α to that we have obtained. In [23] the authors increased the graphene-waveguide separation using a spin-on glass (HSQ) spacer layer, which revealed a dependence of the absorption coefficient on height, *h*, due to the interaction strength of the evanescent field, according to:

$$\alpha(h) = \alpha_0 e^{-2\gamma h} \tag{2}$$

We assign $\alpha_0$ ( = $0.11 dB\mu m^{-1}$) as the experimental value we have obtained for the TE-mode linear absorption coefficient for $h = 0$ and γ ( = $8.5\mu m^{-1}$) is the waveguide evanescent field decay constant determined from a fit to the data of Fig. 4(d) in [23]. Expanding our analysis of the change in peak extinction with $L_g$, to include Eq. (2), we can write a general expression for the resonant signal attenuation in our cavities, $A_g$ ($L_g$, h) induced by the graphene as:

$$A_g\left(L_g, h\right)_{dB} = \left[ER(0) - ER(L_g)\right]_{dB} = \alpha_0 e^{-2\gamma h} L_g \tag{3}$$

A contour plot of $A_g$ as a function of both $L_g$ and *h* is shown in Fig. 4.

Figure 4 reveals that, for $L_g \leq 25\mu m$, the cavity signal attenuation induced by a graphene layer is negligible at large *h* (max 3dB at $h = 0$) but this becomes increasingly significant for longer lengths of graphene, particularly if it is deposited at the waveguide surface. For instance, for $L_g = 150\mu m$, the cavity signal is reduced to half its original value for a graphene height, *h* ~120nm and for this length of graphene deposited at the surface ($h = 0$), a cavity resonance with ER(0) ~17dB (similar to that described in Fig. 2) would be all but quenched. This agrees well with our observations for fully coated racetrack resonators with r > 20μm and $L_c = 13\mu m$ ($L_g = 2\pi r + 2L_c > 152\mu m$), for which the transmission spectra yields no resonances. In order to confirm that the graphene we have deposited sits at the cavity surface, we have carried out a careful analysis, using scanning probe microscopy (not shown here) of a step from the plasma etched substrate to the graphene, which indicates a height, $1 < h \leq 1.5nm$. This is typical for graphene on a (native) silicon dioxide surface, particularly under ambient conditions and indicates that the graphene layer resides at the cavity surface.

The predictive power of our model has important implications for the design of graphene/silicon photonic devices, depending on the target application. For instance, in refractive index sensing applications, where one relies upon being able to measure small shifts in the cavity resonant wavelength, these design rules dictate that small $L_g$ and/or large *h* should be employed to improve the reactivity of the silicon surface without sacrificing the cavity resonance signal. Practically, $L_g$ can be controlled using selective etching to partially coat the race-track cavities with graphene whilst the inclusion of a (low-loss) dielectric spacer layer (such as HSQ) can be used to increase the height, *h* of the graphene above the cavity

#212944 - $15.00 USD Received 27 May 2014; revised 7 Jul 2014; accepted 8 Jul 2014; published 25 Jul 2014

surface. Indeed, control over such spacer layer thickness (at the 10's nm range) has already been demonstrated on silicon Mach-Zehnder type devices [23]. On the other hand, for e.g. photo-detector applications, one requires maximum absorption in the graphene layer and therefore designs should aim for large $L_g$ and/or small $h$. It is worth pointing out that, for TM-mode operation, a different set of curves can be expected due to graphene's polarization sensitive absorption coefficient [22, 25].

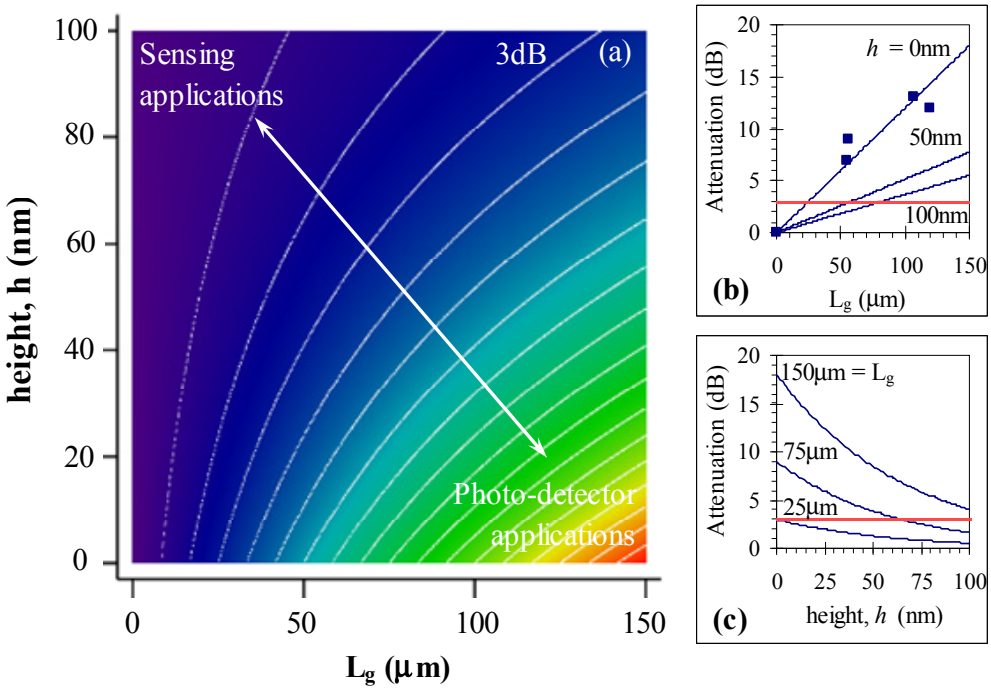


Fig. 4. (a) contour plot of the calculated signal attenuation, $A_g$ (blue – low, red – high, contour lines – 1dB increment) as a function of length, $L_g$ and height, $h$ of graphene over the silicon cavity ring resonator (b) calculated $A_g$ as a function of $L_g$ for specific heights ($h$ = 0, 50, 100nm) along with our measured data (blue squares) and (c) calculated $A_g$ as a function of height for specific lengths ($L_g$ = 25, 75, 150μm). The red dashed lines in (b) and (c) indicate the graphene ($L_g$, $h$) co-ordinates where the cavity resonance signal is attenuated by 3dB

## 4. Conclusions

We have deposited CVD graphene on racetrack type silicon cavity resonators as a route to improving the surface reactivity for bio-molecular and/or gas sensing applications. Measurements and analysis of the transmission spectra for a cavity with no graphene and for graphene integrated cavities reveal a strong quenching of the resonance signal with increasing light-graphene interaction length, which is due to the quasi-TE mode (*in-plane*) absorption in graphene. From these analyses we obtain a value for the graphene linear absorption coefficient, $\alpha_{gTE} = 0.11 \pm 0.01 dB\mu m^{-1}$, which is in excellent agreement with literature values if we assume the graphene intersects the evanescent field of the guided mode at the cavity surface. A model of the cavity resonance signal attenuation for different graphene length and height co-ordinates over such cavities provides design rules for different graphene integrated silicon photonic devices according to the required application.


## Acknowledgments

This work was supported by the Engineering and Physical Sciences Research Council grant EP/K016946/1. NC and AV also acknowledge P. Gorgojo for her assistance.



#212944 - $15.00 USD Received 27 May 2014; revised 7 Jul 2014; accepted 8 Jul 2014; published 25 Jul 2014